Fine Tuning the Emission Properties of Nanoemitters in Multilayered Structures by Deterministic Control of their Local Photonic Environment

Alberto Jiménez-Solano, Juan Francisco Galisteo-López,* and Hernán Míguez*

The emission properties of a light source are known to be dictated by its photonic environment via the local density of radiative states (LDOS).[1] As a matter of fact, one of the goals in the field of nanophotonics is the control of the LDOS in the vicinity of nanoemitters by a judiciously engineered local environment. In doing so, the radiative decay rate of the emitter can be tuned and its quantum yield (QY) improved, paving the way for more efficient light sources. Further, such control is expected to introduce a plethora of nonconventional light sources from threshold-less lasers[2] to single photon sources.[3] Over the past two decades, photonic crystals (PhC) have been eagerly explored as a platform to exert such local control on the photonic environment of nanoemitters. In these systems introducing a periodic spatial variation on the refractive index yields a spectral redistribution of its LDOS which can strongly modulate the spontaneous emission of internal sources being one extreme case its complete inhibition.[2] But the fabrication of systems where a deterministic control on the LDOS can take place poses a challenge: methods that yield large samples amenable to be mass produced often prevent the incorporation of nanoemitters at well-defined positions and thus control on LDOS is lost. On the contrary, fabrication methods which allow placing emitters at desired locations cannot produce large samples and often demand large facilities and are time consuming.

As the dimensionality of the periodicity decreases, the placement of light sources at precise locations of the structure becomes more accessible from the point of view of fabrication, being 1D PhC a clear example. In these systems, emitters can be placed along a plane in the fabrication procedure, where the LDOS is constant. As a matter of fact, 1D PhC can be used as a means to strongly modify the emission dynamics of emitters[4] or to fabricate laser devices in the shape of vertical-cavity surface-emitting lasers.[5] Recently, a new class of 1D PhC has been demonstrated where the layers forming the structure are made of optical-quality films of oxide nanoparticles (NP).[6,7] These systems present two levels of structuration: one at the nanometer scale originating from the size of the NP composing the different layers which creates a highly porous environment that can be infiltrated with polymeric materials or solutions and another one at a scale of hundreds of nanometers dictated by the thickness of the different NP films which determines the photonic environment due to Bragg diffraction. Over the past few years, the potential of these structures as materials for photonic applications has been demonstrated in many examples ranging from UV mirrors[8] to photovoltaic,[9] sensors,[10] or light-emitting devices. Examples of the latter comprise their use as filters to spectrally filter the output of light-emitting diodes (LEDs)[11] and environments to provide optical feedback for efficient optically pumped organic lasers.[12,13]

While the above mentioned examples highlight the potential of nanoporous 1D PhC for optical applications, a precise knowledge of their local photonic environment is essential prior to their incorporation into real life devices. Here, we demonstrate a spatial mapping of the emission properties of nanoemitters as they are placed at different positions across a resonator placed within two porous Bragg stacks. We map both the photoluminescence intensity of the emitters, carrying information on the total field intensity (TFI) at their location, as well as their decay dynamics, dictated by the LDOS. Contrary to other studies of local emission properties in PhC of higher dimensionality, where the lack of control on light source position often demands a statistical single-emitter study[14] or ensemble interpretation[15] where information on the precise photonic environment at a given position is lost, here we are able to combine spin- and dip-coating deposition techniques to place the emitters along a monolayer of constant LDOS and hence observations in a macroscopic measurement can be directly related to changes in the microscopic LDOS. Changes in decay rates below 1% are probed and accounted for by numerical simulations. These results constitute a proof of principle which can be further extended to many 1D periodic structures that could be exploited as components for photonic devices.

The systems under study are porous 1D PhC fabricated through a sequential deposition of thin films of TiO_2 and SiO_2 nanoparticles by dip coating of a clean glass substrate in different sols (see Experimental Section). The final sample consisted of a TiO_2 resonator (thickness 200 nm) surrounded by three TiO_2/SiO_2 bilayers (105/110 nm thick respectively)

A. Jiménez-Solano, Dr. J. F. Galisteo-López, Prof. H. Míguez
Instituto de Ciencia de Materiales de Sevilla
Consejo Superior de Investigaciones Científicas
(CSIC)-Universidad de Sevilla
C/Américo Vespucio 49, 41092 Sevilla, Spain
E-mail: juan.galisteo@csic.es; h.miguez@csic.es
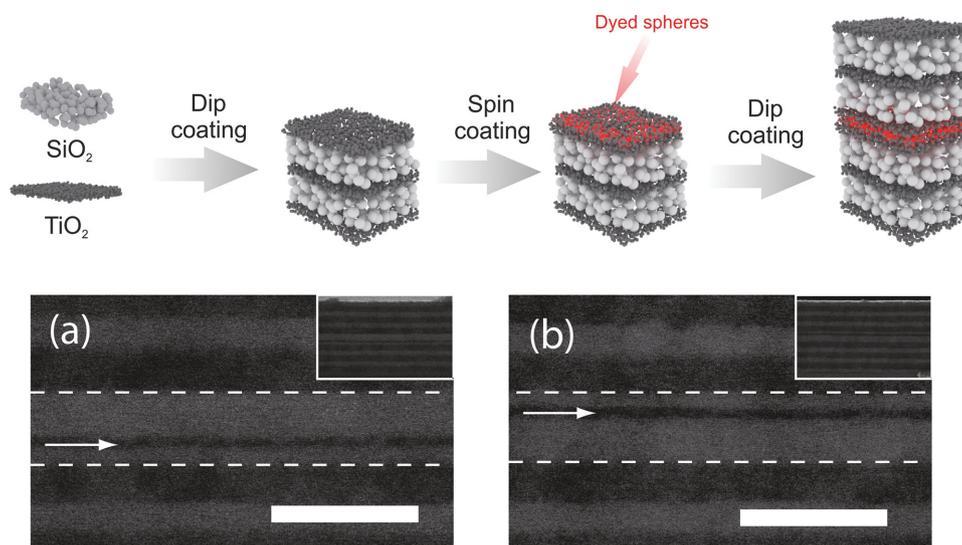
Figure 1. Diagram showing the fabrication procedure of a resonator combining dip and spin coating. a,b) SEM images obtained with backscattered electrons of two samples with a monolayer of spheres (pointed by arrow) placed at two different spatial positions within a resonator (highlighted by dashed lines). Scale bars correspond to 300 nm. Insets show same sample at lower magnification. Dark (bright) regions correspond to SiO_2 (TiO_2) films.

on each side (see **Figure 1**). Nanoemitters in the shape of dye-doped polystyrene (DPS) spheres (Thermo Scientific) with a diameter of 25 nm were included within the resonator by stopping the dip coating at a given stage of the growth and depositing a mixture of TiO_2 NPs and DPS nanospheres by spin coating. This yielded a monolayer of nanoemitters whose position within the resonator could be controlled by interrupting the dip coating at different stages of the process. The resulting DPS monolayer was embedded within a TiO_2 film, which restricts its proximity to the resonator edges to 50 nm (Figure 1). Employing this combination of spin- and dip-coating techniques, samples where the emitting layer was placed at seven different positions within the resonator were fabricated.

The ratio DPS/TiO_2 in the mixture to be dip-coated was optimized in order to generate an emitting layer which could stand further dip-coating steps and yield a photoluminescence (PL) signal that can be detected. As mentioned above, the final conditions led to a DPS monolayer embedded within a TiO_2 film. The position of the spheres within the resonator can be extracted from field-emission scanning electron microscopy (FE-SEM) images obtained with backscattered electrons where it appears as a dark band within a lighter one corresponding to the TiO_2 film (see Figure 1). Reference samples were produced by depositing a TiO_2 layer by dip coating followed by spin coating deposition of a mixture of DPS and TiO_2 on a clean glass substrate.

Figure 2a shows the spatial and spectral dependence of the TFI together with the reflectance spectrum simulated employing a transfer matrix code (see Experimental Section) for a sample whose structural parameters were extracted from FE-SEM images. In the simulation, light enters the sample from $X = 0$ nm and the TFI is concentrated within the cavity for those frequencies corresponding to the resonant mode. In a first stage, we measured the PL for samples having a monolayer of emitting nanospheres at different positions within the resonator. Evident changes in PL, as compared to a reference sample with a constant refractive index, are dictated by the fractional LDOS[16] which accounts for those modes allowed for propagation along the detection direction. As the emitter layer is scanned across the defect we see both, regions of enhanced (Figure 2b) and suppressed (Figure 2c) PL. If we plot the ratio of the PL in the sample and in a reference system for a wavelength matching the defect state for all positions of the nanoemitter monolayer within the resonator (Figure 2d), we see a continuous evolution from enhanced PL at the resonator edges toward a minimum at the center. As expected, these measurements show a strong dependence of the PL with emitter position[16] which could not be observed if the emitters were distributed throughout the entire defect. As we have found variations of 4% in the resonator width of the different fabricated structures all data are presented in terms of relative position X_R within the TiO_2 cavity for comparison, where 0/1 corresponds to the edges and 0.5 to the center.

Together with the experimental PL ratios we have extracted the TFI at the same relative positions within the resonator at which nanoemitters were placed, for a wavelength corresponding to the defect state at normal incidence (Figure 2e). While the overall trend is identical for experimental PL ratio and simulated TFI, discrepancies in absolute values are evident. Besides the fact that structural imperfections may introduce losses in the experimental case, the TFI cannot be directly compared with PL variations. The TFI shows the field distribution within the sample when illuminated with an external plane wave and is thus influenced by the coupling of the incoming beam to the sample. On the other hand, light emitted from the monolayer of nanoemitters cannot be described as a plane wave and a factor dealing with the outcoupling of the emitted light should be considered. Nevertheless, the overall trend is well reproduced.

Next, time-resolved PL measurements were carried out on the same samples with monolayers of nanoemitters placed
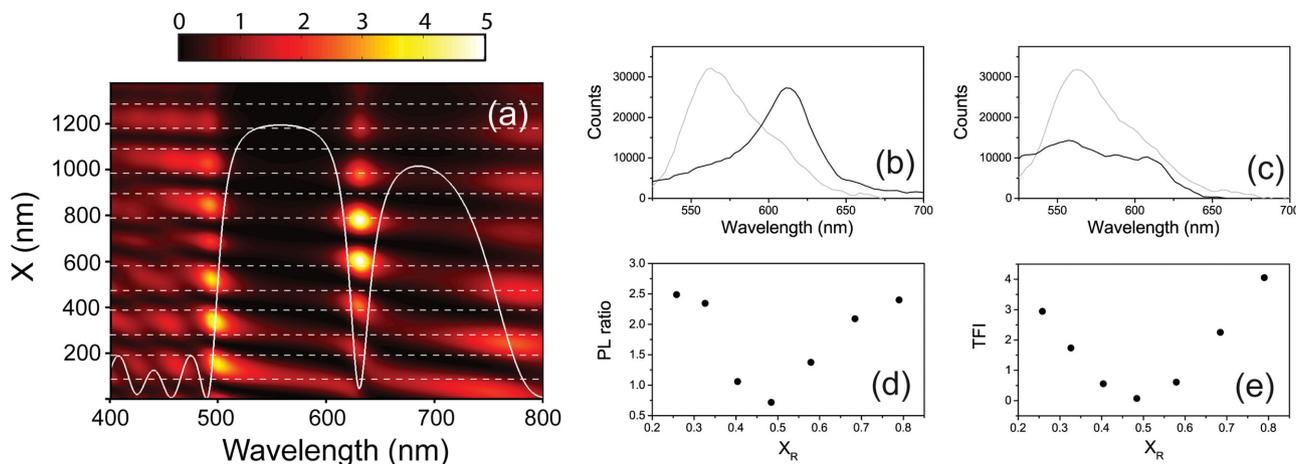
Figure 2. a) Total field intensity of a sample illuminated with a plane wave impinging from X = 0 together with its reflectance spectrum (white line). Dashed lines denote the interfaces between NP layers. b,c) PL spectra of a reference sample (gray curve) and samples (black curve) with a monolayer of DPS spheres placed at one edge and at the center of the resonator respectively. d) Ratio between the PL in a reference sample and resonators containing a DPS sphere layer at different relative positions within the cavity for a wavelength corresponding to the resonant mode at normal incidence $\lambda_0 = 620$ nm. e) Total field intensity for λ_0 at the relative positions within the simulated resonator found in the fabricated samples.

at different positions within the resonator. PL was collected over a 5 nm spectral window (selected with a monochromator) centered at λ_0. Contrary to angular PL measurements discussed earlier, dynamic measurements carry information only of the local photonic environment of the sample, given that the chemical environment of the emitters remains constant as in our case, since dye molecules encapsulated within the polystyrene (PS) spheres sense the same chemical environment in the samples and the reference system.

Experimental decay curves were fitted with a normal distribution of decay rates rather than a single rate (see **Figure 3**a). An excellent fit with χ^2 in the 1.1–1.4 range was obtained in all cases. While in previous analysis of decay dynamics in 3D PhC the presence of a distribution of decay rates was associated with an ensemble of emitters located at different unit cell positions and hence probing a broad distribution of LDOS[17] in our case it comes from the intrinsic narrow distribution characteristic of these spheres[18] and the fact that although they are located at planes of constant LDOS they have a finite diameter (25 nm) which means that LDOS is averaged over that distance. In other words, the sphere diameter sets the spatial resolution of this measurement. Such a resolution is remarkable taking into account that we are performing a macroscopic measurement with a pump beam with a 0.9 cm^2 diameter. Further broadening of the decay distribution due to sample inhomogeneity was ruled out as no change in the reflectance spectra was observed as a probe beam with a 0.5 mm spot of a microscope-coupled Fourier transform spectrophotometer (Bruker IFS-66 FTIR) was scanned across the region of interest.

The above dynamic measurement was performed for all fabricated samples. The lifetime was measured at the wavelength corresponding to the cavity mode at normal incidence so that enough PL signal was obtained. As mentioned earlier, such wavelength had a 4% variation between different samples due to small deviations inherent to the fabrication process. Figure 3b shows the mean value of the lifetime distribution τ_0 for samples having a monolayer of

nanoemitters placed at different relative positions within the resonator. Here, a clear trend is observed with faster decays taking place close to the resonator edges. The full width at
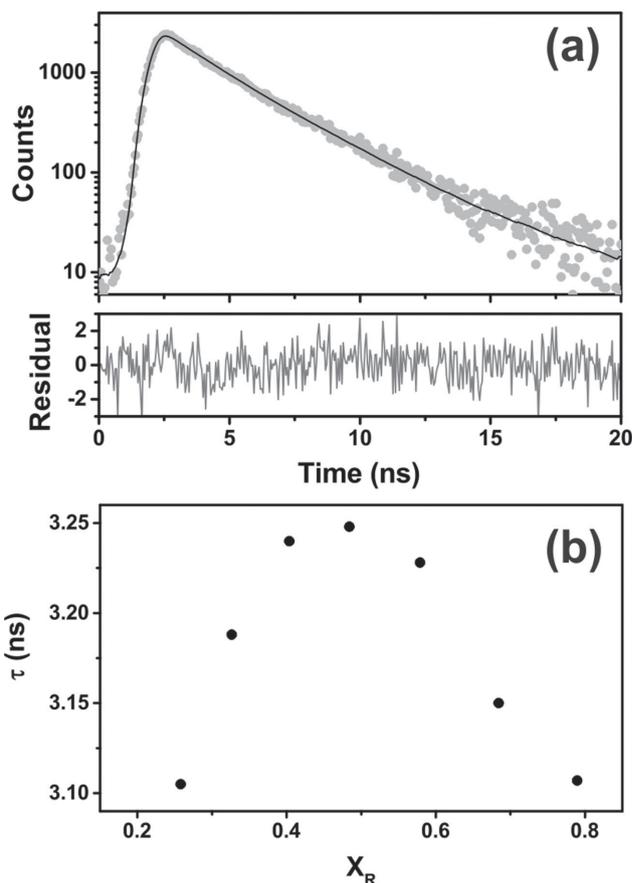
Figure 3. a) Decay curve (gray dots) for a sample with a monolayer of spheres placed at the resonator's center together with a fit (black line) assuming a distribution of lifetimes. Bottom panel shows the residual of the fit. b) Mean value of the lifetime distribution for seven resonators having a monolayer of spheres placed at different relative positions.
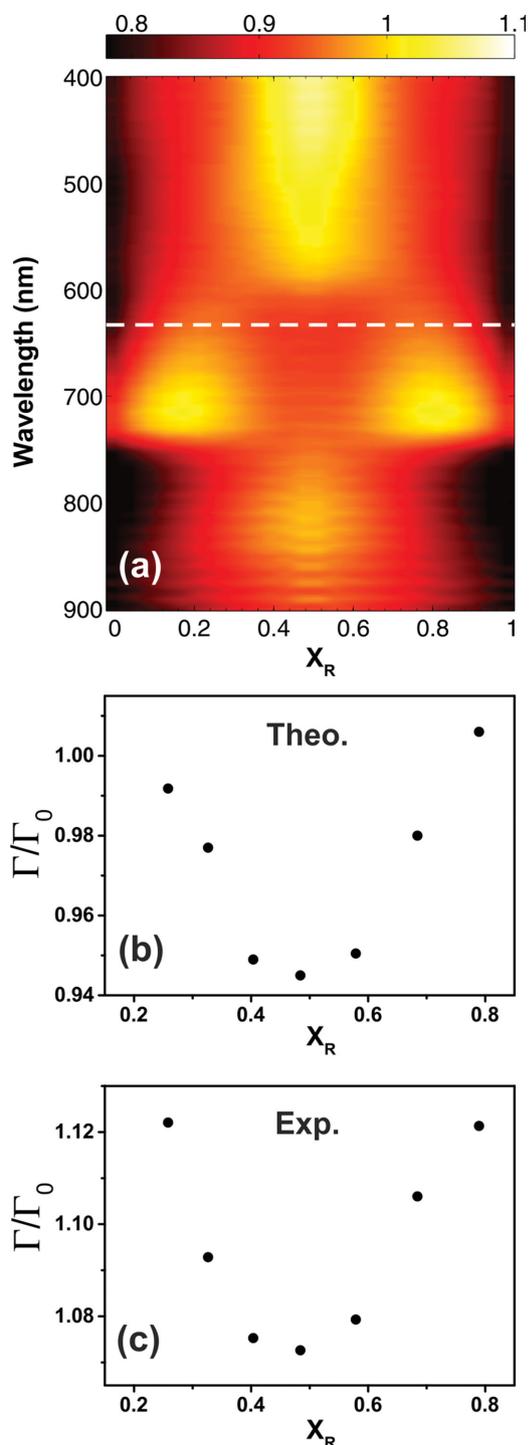
Figure 4. a) Calculated decay rate as a function of wavelength and relative position of an isotropic dipole within a resonator. White dashed line represents the spectral position of the cavity mode at normal incidence. b,c) show, respectively, theoretical and experimental values for a wavelength corresponding to the defect state at different relative positions within the resonator.

half-maximum (FWHM) of the lifetime distribution had a value of 1 ± 0.15 ns in all cases.

Experimental results were simulated with numerical finite difference in time domain (FDTD) calculations (see Experimental Section). **Figure 4**a shows a spatial map of the decay dynamics of an isotropically emitting dipole placed at different relative positions within the resonator. The decay rate of the dipole, Γ, is normalized to that of a reference dipole in a homogeneous medium having the refractive index of the TiO_2 cavity, Γ_0. Changes in the decay dynamics of the emitter can be directly related to changes in the LDOS within the resonator according to Fermi's Golden Rule.[1] The dynamics of the emitter are seen to vary across the resonator as previously predicted in ref. [19] following an analytical approach. The spectral position of the cavity mode at normal incidence is highlighted with a dashed line. We have extracted the ratio Γ/Γ_0 at the different relative positions within the cavity corresponding to the fabricated samples (Figure 4b) for comparison with the experimentally measured (Figure 4c).

Although the agreement between theory and experiment is outstanding in terms of the spatial trend and the relative changes observed in the decay rate ratio, some discrepancies are present. Experimental values are 10% larger in general than theoretical ones. The possibility of the DPS sphere layer (not considered in the simulation) modifying the resonator was ruled out as the refractive indices of PS (1.59) and the TiO_2 NPs film (1.61) are rather similar as compared to the SiO_2 films (1.2). The origin of this discrepancy is likely the reference decay rate used in each case to extract the presented ratio. While in the simulated system a large TiO_2 matrix surrounding the emitting nanospheres was considered ($4 \times 4 \times 2.4$ μm), experimentally a nanostructured TiO_2 thin film (thickness ≈50 nm) embedding the spheres was used. The effective index surrounding the spheres in the experimental reference system is therefore lower than in the simulated case, which could account for a faster reference decay rate and thus an overall larger Γ/Γ_0 ratio.[1]

While emitters are usually introduced within cavities to enhance or decrease their emission dynamics, it is evident that both effects can be achieved within a given structure simply by changing the emitter's position within the resonator. Further, by changing the dipole emission wavelength by a few tens of nanometers a complete different trend can be observed (see Figure 4a) where the maximum decay rate lies at the center rather than the edges of the resonator. These changes in the measured total decay rate $\Gamma = \Gamma_R + \Gamma_{NR}$ are due to modifications in the radiative component (Γ_R), as the nonradiative one (Γ_{NR}) remains unchanged, and also influence the QY of the emitters given by the radiative component of the total decay rate $\Gamma_R/(\Gamma_R + \Gamma_{NR})$. But such control on the emission dynamics of a dipole can only be exerted if its location within the resonator can be tailored with nanometer precision. Further, although a nanoemitter with a distribution of decay rates is employed in the present case, it is worth noting that changes in decay dynamics with a resolution below 1% can be probed by monitoring changes in the mean value of the distribution.

While this is a proof of principle on how the local photonic environment of porous 1D PhC can be probed in the nanoscale employing a macroscopic measurement, its use can be extended to other systems where the potential to fabricate devices has been demonstrated such as aperiodic chirped structures.[12] Contrary to other single-emitter approaches on 2D[14] or 3D systems,[18] or ensemble-averaged

measurements[15] where strong changes in the decay dynamics of nanoemitters were observed without a precise knowledge on emitter position, here small (<1%) variations of the decay rate can be probed and directly related to emitter positions separated by a few tens of nanometers.

We have studied with nanometric spatial resolution the local photonic environment of porous 1D PhC containing optical microcavities. By introducing with a large degree of control a monolayer of organic emitters in the shape of dye doped polymeric nanospheres within the resonator, relative variations in their decay rate below 1% have been measured and associated with changes in the local photonic environment within the cavity. As mentioned above, deterministically modifying the radiative properties of the emitters in such small steps implies a fine tuning of their QY. While the spatial resolution is dictated by the sphere diameter (i.e., 25 nm) in principle the resolution is only limited by the pore size of the structure so one could resort to quantum-dots (QDs) or nanophosphors[20] where spatial resolution could be reduced down to a few nanometers. Further, the present study can be extended to other layered nanoporous structures whose potential as optical elements such as cavity-less laser sources has already been demonstrated.[13]

Experimental Section

Sample Fabrication: Nanoporous 1D PhC were prepared by successive dip coating of nanocolloids of TiO_2 (synthesized using a procedure previously described[7], SiO_2 (LUDOX TMA, Aldrich), and dye-doped luminescent (absorption/emission maxima at 534 and 570 nm, respectively) polystyrene spheres with a 25 nm diameter (Thermo Scientific). The TiO_2/SiO_2 NPs have an irregular/spherical shape[21] with average sizes of 7/30 nm and they form thin films of optical quality with an internal arrangement consisting of a random porous network.[22] The TiO_2 and SiO_2 sols were deposited over zero fluorescence microscope slides (Proscitech) using a dip-coater (Nadetech ND-R) with a withdrawal speed of 110 mm min^{-1}. Both suspensions were diluted in methanol with concentrations of 1 wt%. Each layer comprising the structure is deposited in several steps of the same suspension (to increase the thickness layer resolution) with a waiting time of 10 s between dips to ensure solvent evaporation.

The monolayer of DPS spheres was deposited within the optical cavity of the PhC by spin coating (Laurell WS-400) using 100 µL of a 2:8 mixture of TiO_2 NP and DPS spheres (both 1 wt%) with an acceleration ramp of 11 340 rpm^{-1} and a final rotation speed of 1500 rpm. The deposition of the monolayer was completed in 60 s. The choice for the DPS/TiO_2 mixture allowed us to introduce the dyed spheres directly within the cavity in a controlled and homogeneous manner (as seen in the SEM images) in a way that they could stand subsequent dip-coating steps needed to grow the remaining photonic structure.

Numerical Simulations: The optical response of the photonic structure (i.e., reflectance/transmittance), as well as the total field intensity, were simulated with full wave vector calculations performed by using a transfer matrix formalism implemented in a code written in MatLab following the standard transfer matrix formulation.[23] The local photonic environment within the resonator was simulated using a commercial FDTD software.[24] For the latter, a map of the decay dynamics of different dipoles placed within the resonator and separated 10 nm was carried out. Decay rates Γ were extracted from the imaginary component of the Green's function at the dipole location.[25] In order to simulate an isotropic dipole, the average between three orthogonal dipoles was obtained. Broadband emitting sources were simulated with a center frequency similar to that of the dyes embedded within the PS spheres. The refractive indices were estimated carrying out an analysis of the structure by simulating the reflectance spectra of the sample. In order to do so, the above mentioned code based on a combination of a transfer matrix method (to calculate the reflectance of each sample) and a genetic algorithm to search for the optimum fitting (maximizing the r^2 value between the experimental and simulated spectra) was developed. The layer thicknesses were taken from the SEM analysis. From the obtained indices a porosity slightly above 50% for the nanoporous TiO_2 and SiO_2 films were obtained (corresponding to effective refractive indices of 1.61 and 1.2 for the TiO_2 and SiO_2 films, respectively).

Optical Characterization: The photoluminescence spectra of the DPS spheres in different samples was collected at near normal incidence (11.25°) using a commercial spectrometer (Fluorolog-3 Horiba Jobin Yvon) upon optical pumping with a fiber coupled tunable laser (Fianium SC400) delivering low power (mW) 900 ps long pulses. The pump conditions (normal incidence and $\lambda_{pump} = 480$ nm) were chosen so that no photonic effect (forbidden frequency intervals or band edges) affected the optical excitation. A built-in time correlated single photon counting module (Fluorohub) was used for time-resolved measurements.

Structural Characterization: FE-SEM images of cross sections of the films were taken with a Hitachi S5200 microscope operating at 5 kV.

[1] L. Novotny, B. Hecht, *Principles of Nano-Optics*, Cambridge University Press, USA **2006**.

[2] E. Yablonovitch, *Phys. Rev. Lett.* **1987**, *58*, 2059.

[3] J. Vučković, D. Fattal, C. Santori, G. S. Solomon, Y. Yamamoto, *Appl. Phys. Lett.* **2003**, *82*, 3596.

[4] G. Björk, S. Machida, Y. Yamamoto, K. Igeta, *Phys. Rev. A* **1991**, *44*, 669.

[5] F. Koyama, *J. Lightwave Technol.* **2006**, *24*, 4502.

[6] D. Lee, M. F. Rubner, R. E. Cohen, *Nano Lett.* **2006**, *10*, 2305.

[7] S. Colodrero, M. Ocaña, A. R. González-Elipe, H. Míguez, *Langmuir* **2008**, *24*, 9135.

[8] J. R. Castro-Smirnov, M. E. Calvo, H. Míguez, *Adv. Funct. Mater.* **2013**, *23*, 2805.

[9] M. Anaya, M. E. Calvo, J. M. Luque-Raigón, H. Míguez, *J. Am. Chem. Soc.* **2013**, *135*, 7803.

[10] B. Auguié, M. C. Fuertes, P. C. Angelomé, N. López-Abdala, G. J. Soler-Illia, A. Fainstein, *ACS Photon.* **2014**, *1*, 775.

[11] D. P. Puzzo, M. G. Helander, P. G. O'Brien, Z. Wang, N. Soheilnia, N. Kherani, Z. Lu, G. A. Ozin, *Nano Lett.* **2011**, *11*, 1457.

[12] D. P. Puzzo, F. Scotognella, M. Zavelani-Rossi, M. Sebastian, A. J. Lough, I. Manners, G. Lanzani, R. Tubino, G. A. Ozin, *Nano Lett.* **2009**, *9*, 4273.

[13] F. Scotognella, D. P. Puzzo, A. Monguzzi, D. S. Wiersma, D. Maschke, R. Tubino, G. A. Ozin, *Small* **2009**, *5*, 2048.

[14] T. Kaji, T. Yamada, S. Ito, H. Miyasaka, R. Ueda, S. Inoue, A. Otomo, *J. Am. Chem. Soc.* **2012**, *135*, 106.

[15] P. Lodahl, A. F. van Driel, I. S. Nikolaev, A. Irman, K. Overgaag, D. Vanmaekelbergh, W. L. Vos, *Nature* **2004**, *430*, 654.

[16] M. Barth, A. Gruber, F. Cichos, *Phys. Rev. B* **2005**, *72*, 085129.

[17] A. F. van Driel, I. S. Nikolaev, P. Vergeer, P. Lodahl, D. Vanmaekelbergh, W. L. Vos, *Phys. Rev. B* **2007**, *75*, 035329.

[18] R. Sapienza, P. Bondareff, R. Pierrat, B. Habert, R. Carminati, N. F. van Hulst, *Phys. Rev. Lett.* **2011**, *106*, 163902.

[19] N. Dantz, R. Waldhäusl, A. Bräuer, R. Kowarschik, *J. Opt. Soc. Am. B* **2002**, *19*, 412.

[20] F. Wang, X. Liu, *Chem. Soc. Rev.* **2009**, *38*, 976.

[21] S. Colodrero, A. Forneli, C. López-López, L. Pellejà, H. Míguez, E. Palomares, *Adv. Funct. Mater.* **2012**, *22*, 1303.

[22] N. Higalgo, C. López-López, G. Lozano, M. E. Calvo, H. Miguez, *Langmuir* **2012**, *28*, 13777.

[23] P. Yeh, *Optical Waves in Layered Media*, Wiley, New York **1988**.

[24] Lumerical Solutions Ltd., www.lumerical.com, accessed: September 2014.

[25] C. van Vlack, S. Hughes, *Opt. Lett.* **2012**, *37*, 2880.